Journal of Nuclear Medicine, published on July 12, 2018 as doi:10.2967/jnumed.118.213678

Assessment of Physiological Intracranial Calcification in Healthy Adults Using 18F-NaF PET/CT

Abdullah Al-Zaghal,[1], Siavash Mehdizadeh Seraj,[1], Thomas J. Werner,[1], Oke Gerke,[2], Poul F. Høilund-Carlsen,[2,3], Abass Alavi,[1]

Affiliations

1. Department of Radiology, Hospital of University of Pennsylvania, PA, USA
2. Department of Nuclear Medicine, Odense University Hospital, Odense, Denmark
3. Department of Clinical Research, University of Southern Denmark, Odense, Denmark

Corresponding Author

Abass Alavi

3400 Spruce St, Philadelphia, PA 19104

Office number: 215-662-3069

Fax number: 215-573-4107

Email address: abass.alavi@uphs.upenn.edu

First Author

Abdullah Al-Zaghal

Research fellow

3400 Spruce St, Philadelphia, PA 19104

Telephone number: 215-834-3014

Fax number: 215-573-4107

Email address: abdullah.alzaghal@uphs.upenn.edu

Word Count 4045

Funding

This study was funded by the Anna Marie and Christian Rasmussen's Memorial Foundation, University of Southern Denmark, Odense, Denmark, and the Jørgen and Gisela Thrane's Philanthropic Research Foundation, Broager, Denmark.

Short running title

Intra-cranial calcification/NaF PET

ABSTRACT

The aim of this research study was to determine the role of ^{18}F-Sodium fluoride (NaF) PET/CT imaging in the assessment of physiologic molecular calcification in the intra-cranial structures. We also examined the association of NaF accumulation with age as well as Hounsfield unit (HU) in certain anatomical sites that are known to calcify with normal aging.

Methods: A total of 78 healthy subjects from the Cardiovascular Molecular Calcification Assessed by ^{18}F-NaF PET/CT (CAMONA) clinical trial (38 females and 40 males) were included in this retrospective study. The mean age was 45.28 ± 14.15 years (21-75). Mean standardized uptake values (SUVmean) was used to measure NaF accumulation in the choroid plexus and epithalamus (pineal gland and habenula). Maximum HU was also measured for each ROI. Correlation analysis was conducted to assess the association between parameters.

Results: Mean SUVmean was 0.42 ± 0.26 in the right choroid plexus, 0.39 ± 25 in the left choroid plexus, and 0.23±0.08 in the epithalamus. Significant positive correlations were present between NaF uptake and age in the right choroid plexus (r=0.61, p<0.0001), left choroid plexus (r=0.63, p<0.0001), and epithalamus (r=0.36, p=0.001). NaF uptake significantly correlated with HU in the right choroid

plexus (r=0.52, p<0.0001), left choroid plexus (r=0.57, p<0.0001), and epithalamus (r=0.25, p=0.03).

Conclusion: NaF could be used in the assessment of physiological calcification in several intracranial structures. We report significant associations between NaF uptake and aging as well as HU in the calcified choroid plexus and epithalamus. Our findings further support the growing interest to utilize NaF for detecting extra-osseous, molecular calcification, and this powerful probe has potential applications in the evaluation of various age-related, neurodegenerative brain processes.

Keywords:

NaF, choroid plexus, pineal gland, brain calcification, PET

INTRODUCTION

^{18}F-labeled Sodium fluoride (NaF) was first employed as a molecular imaging probe in 1962 by Blau et al (*1*) and was approved by the U.S Food and Drug Administration (FDA) in 1972 for routine assessment of osseous disorders including metastasis from various malignancies. NaF gained a great deal of popularity as an excellent bone-seeking agent due to its high skeletal uptake and rapid blood clearance from the circulation following its intravenous administration. However, due to lack of appropriate imaging instruments (positron emission tomography – PET), efforts were made to synthesize compounds that could be used with conventional nuclear medicine techniques. Therefore, routine use of NaF declined since conventional gamma cameras were unable to detect the high energy positron annihilation following ^{18}F decay. The introduction of modern positron emission tomography (PET) scanners and the increased availability of NaF have resulted in a renewed interest in this tracer. Its sensitivity in detecting benign and malignant osseous disorders is significantly higher than that of ^{99m}Technetium-labeled phosphates (*2-4*).

Extra-osseous accumulation of NaF as a marker of soft tissue calcification has been reported in many settings (*5,6*). NaF uptake in the arterial wall of arteries such

as the aorta, carotid and coronary arteries indicate an active calcifying atherosclerotic plaque (*7-9*). NaF is also taken up in the extra-osseous microscopic calcification, dystrophic calcification, and calcified metastatic lesions (*10-13*).

Intracranial calcification is a common neuro-imaging finding in otherwise asymptomatic, normal individuals or in patients with a wide range of underlying maladies such as neurological, metabolic, infectious, hemorrhagic, neoplastic or other disorders (*14*). Choroid plexus calcification is very common finding, usually in the atrial portions of the lateral ventricles. Pineal region calcification is known to be present histologically from fetal life to adulthood. Idiopathic intracranial calcification is defined as the deposition of calcium within brain parenchyma in the absence of neurological deficits or an apparent underlying pathological cause (*15*). During the human life span, the choroid plexus, pineal gland, and habenula tend to accumulate physiologic calcifications.

The purpose of this study was to determine the use of NaF PET in the detection and characterization of active calcification in intra-cranial structures. We also investigated the possible association between NaF uptake and age as well as HU at the sites selected for this research project.

MATERIALS AND METHODOLOGY

NaF PET/CT scans used in this retrospective study are part of the 'Cardiovascular Molecular Calcification Assessed by ^{18}F-NaF PET/CT" (CAMONA) protocol. CAMONA is a prospective trial and was approved by the Danish national committee on biomedical research ethics, registered at ClinicalTrials.gov (NCT01724749), and conducted from 2012 to 2016 in accordance with the Declaration of Helsinki. Details of the CAMONA study were previously published by Blomberg BA, et al. (*16*).

Subject Selection

The CAMONA study included 89 healthy volunteers who were recruited from the general population by local advertisement or from the blood bank of Odense University Hospital, Denmark. Negative history of cardiovascular disease, oncologic disease, chronic inflammatory disease, autoimmune disease, immunodeficiency syndromes, alcohol abuse, illicit drug use, or any prescription medication were inclusion criteria for healthy volunteers. Active smokers and pregnant ladies were excluded. Adults were preselected by sex and age to ensure a balanced inclusion of males and females aged 20–29, 30–39, 40–49, 50–59, and 60 years or older.

Framingham Risk Score (FRS) was used to evaluate the modifiable cardiovascular risk factors and only subjects with score below the upper limits of the recommended levels were included; systolic blood pressure below 160 mm Hg and a diastolic blood pressure below 100 mm Hg, total serum cholesterol below 6.2 mmol/L, and glycated hemoglobin (HbA1c) below 48 mmol/L (*17*). Further detailed description of the healthy subjects of the CAMONA study were previously published by Blomberg BA, et al. (*18*).

In the current study, 6 subjects were excluded as their scans were not available within our lab database. Another 5 subjects were excluded due to motion artifact that degraded image quality and prevented optimal images analysis. A total of 78 healthy subjects, 38 females and 40 males, were included, mean age was 45.28 ± 14.15, range 21 – 75. (Table 1). The Danish national committee on biomedical research ethics approved this study and all subjects signed a written informed consent.

Study Design

Study participant were evaluated by blood pressure measurements, blood chemistry testing, Framingham risk score (FRS), ^{18}F-NaF PET/CT imaging. Information regarding smoking habits, family history of CVD, and prescription medication were collected through questioners. Three blood pressure measurements were done for each patient with an interval of 30 minutes while resting in supine position. The average of last two systolic and diastolic measurements were recorded. Blood chemistry tests included fasting total cholesterol, serum low-density lipoprotein (LDL) cholesterol, high-density lipoprotein (HDL) cholesterol, fasting serum glucose, HbA1c, serum creatinine, and the Modification Diet and Renal Disease (MDRD) estimated glomerular filtration rate (eGFR). SCORE % was calculated for each subject based on gender, age, total serum cholesterol, serum HDL cholesterol, systolic blood pressure, and smoking status.

NaF PET/CT scans were performed according to the previously published methodology by Blomberg BA (*19*). In Summary, NaF PET/CT imaging was performed on integrated PET/CT scanners (GE Discovery 690, VCT, RX, and STE (General Electric, Chicago, Illinois, USA)) with comparable spatial resolutions. PET images were obtained 90 minutes after the intravenous administration of 2.2 MBq of ^{18}F-NaF/kg of body weight. The acquisition time per bed position was 2.5

minutes. Total body PET images were acquired in 3D-mode and reconstructed into coronal, transverse, and sagittal slices by an iterative reconstruction algorithm (GE VUE Point). Corrections were applied for attenuation, scatter, random coincidences, and scanner dead time. For attenuation correction and anatomic orientation, low-dose CT imaging (140 kV, 30-110 mA, noise index 25, 0.8 seconds per rotation, slice thickness 3.75 mm) was performed. Total body PET images were acquired in 3D-mode and reconstructed into coronal, transverse, and sagittal planes by an iterative reconstruction algorithm (GE VUE Point).

Image Analysis

Osirix MD v 9.0 (DICOM viewer and image-analysis program, Pixmeo SARL; Bernex, Switzerland) was used for the analysis of fused PET/CT images. Three fixed-size spherical regions of interest (Volume = 1.5 cm^3, Diameter = 1.42 cm) were drawn to encompass the calcified choroid plexus in the inferior horn of the lateral ventricle in each cerebral hemisphere and the epithalamus (including both the pineal gland and habenula) (Fig. 1). SUVmean and maximum HU were measured for each ROI.

Statistical Analysis

Correlation analysis by means of Pearson correlation coefficients and scatterplots was performed to investigate the relation of age with NaF uptake and maximum HU values. The association between NaF uptake and maximum HU was also investigated by correlation analysis. Exploratory multivariable linear regression was applied for all endpoints using all available demographic data (additional online data supplement 1). Due to the limited sample size, the number of explanatory variables was reduced by application of variance inflation factor analysis first and backward variable selection (with p_{stay}=0.7) thereafter, but age and gender were maintained irrespectively of their p-values. A two-tailed P value below 0.05 was regarded statistically significant. Statistical analysis was conducted using Stata/MP 15.0 (StataCorp, College Station, Texas 77845 USA).

RESULTS

Mean SUV was 0.42 ± 0.26 in the right choroid plexus, 0.39 ± 0.25 in the left choroid plexus, and 0.23 ± 0.08 in the epithalamus. The average of maximum HU was 148 ± 66.01 in the right choroid plexus, 141 ± 61.31 in the left choroid plexus, and 235 ± 130.69 in the epithalamus.

Significant positive correlations were present between NaF uptake and age in the right choroid plexus ($r = 0.61$, $p < 0.0001$), left choroid plexus ($r = 0.63$, $p < 0.0001$), and epithalamus ($r = 0.36$, $p = 0.001$). HU values also had a positive correlation with aging in both the right ($r = 0.43$, $p = 0.0001$) and left ($r = 0.40$, $p = 0.0003$) choroid plexus, but not in the epithalamus ($r = 0.19$, $p = 0.09$) (Fig. 2). Exploratory multivariable linear regression supported the statistically significant influence of age on NaF uptake and HU values after adjustment for demographic variables (Additional Online Data Supplement 1).

Significant positive correlations were observed between NaF uptake and HU in the right choroid plexus ($r = 0.52$, $p<0.0001$), left choroid plexus ($r = 0.57$, $p < 0.0001$), and epithalamus ($r = 0.25$, $p = 0.03$) (Fig. 3).

DISCUSSION

Idiopathic intracranial calcification is thought to be related to normal physiological aging and neurodegenerative processes (*20*). It is most commonly found in the choroid plexus, pineal gland, habenula, and dura matter. It is present in 50-70% of adults above the age of 30 years and its incidence increases with age (*21,22*), but it is not uncommon to encounter these finding in young adolescents (*23,24*).

Hydroxyl-apatite ($Ca_{10}[PO_4]_6[OH]_2$) is a major component of calcified intracranial lesions (*25,26*). The 18F-Fluorine ion of NaF exchanges with hydroxyl ions (OH-) on the surface the hydroxyapatite matrix to form fluoro-apatite (*27*). The rate of NaF accumulation depends on the number of binding sites on the surface of hydroxyl-apatite available to react with 18F (*28*). Any anabolic or catabolic process that alters calcium metabolism affects the hydroxyl-apatite surface area, and thus, increases the degree of availability of binding sites, consequently resulting in higher NaF uptake (*29-31*).

Our results showed that NaF-PET could detect and semi-quantify calcium metabolism and its turnover in calcified choroid plexus and epithalamus. We also found significant positive associations between aging and NaF accumulation as well

as HU values in the choroid plexus and epithalamus. NaF accumulation in the regions selected for this study had a significant positive correlation with HU values.

Kwak et al. retrospectively studied 2,877 cranial computed tomography (CT) scans and noted a strong association between the calcification of choroid plexus and pineal gland with normal aging (*32*,*33*). Whitehead et al. examined head CT scans of 500 subjects in their first decade of life and reported a correlation between choroid plexus and pineal gland calcification with age (*34*).

In the population examined, calcification in the epithalamus had higher maximum HU values than that seen in the choroid plexus on CT images. However, the choroid plexus had higher NaF uptake on PET. This may indicate that calcium deposits in the pineal gland were more mature and less metabolically active than the calcification of the choroid plexus. This consolidates the role of PET as a functional imaging modality that reflects the metabolic activity of the investigated organ in contrast to other structural imaging modalities. Pathological studies suggested that the architecture of pineal gland calcifications does not change with age (*35*).

Imaging studies are routinely used in the evaluation of brain calcifications and its associated disorders. Non-enhanced CT scanning is the most commonly used

modality to image brain calcification; calcium deposits have a distinct hyper-dense appearance on CT (*36*,*37*). Calcifications have variable signal intensity on T1-weighted, and T2-weight images. However, iron and calcium deposition in the basal ganglia both have a hypo-intense signal on T2-weight images (*38*), making conventional magnetic resonance imaging (MRI) less reliable than CT in detecting calcifications (*39*). Susceptibility-Weighted Imaging (SWI) has improved the ability of MRI in detecting brain calcification (*40*). The sensitivity of Ultrasound for detecting intracranial calcification is highly comparable to that of CT in early childhood, but it is only feasible to perform in newborns before the closure of the fontanelles which occurs by the 18th month of age (*41*,*42*). Plain radiography is not a reliable modality to detect intracranial calcification, but extensive calcifications could be seen on radiographs as opaque lesions similar to that in the pineal gland or the falx.

Our study was limited by the imaging protocol; images were acquired 90 minutes after administration of NaF instead of the routine 60 minute-protocol, however, these scans originate as stated from the CAMONA project, which deals with molecular arterial calcification, whereas the SNM guideline is for NaF PET/CT bone scans. Molecular imaging with PET to detect intracranial calcification is an important domain of research and may not replace the established methods in the

near future. However, as the experience with this powerful approach becomes substantial, NaF-PET may play a major role in the evaluation of the metabolic activity of calcified brain lesions.

CONCLUSION

Based on the scientific data that we have described in this article, NaF could be used in the assessment of physiological calcification in several intracranial structures. We report a significant association between NaF uptake and aging as well as HU in the calcified choroid plexus and epithalamus. Our findings further support the growing interest to utilize NaF for detecting extra-osseous, molecular calcification and this powerful probe has potential applications in the evaluation of various age-related, neurodegenerative brain calcifications.

ACKNOWLEDGEMENTS

We thank the staff of the CAMONA study and the study participants for their valuable contributions.

DISCLOSURE

This study was funded by the Anna Marie and Christian Rasmussen's Memorial Foundation, University of Southern Denmark, Odense, Denmark, and the Jørgen and Gisela Thrane's Philanthropic Research Foundation, Broager, Denmark.

CONFLICTS OF INTEREST

The authors declare that they have no conflict of interest.

ETHICAL APPROVAL

All procedures performed in studies involving human participants were in accordance with the ethical standards of the institutional research committee and with the principles of the 1964 Declaration of Helsinki and its later amendments or comparable ethical standards.

INFORMED CONSENT

Informed consent was obtained from all individual participants included in the study.

REFERENCES

1- Blau M, Nagler W, Bender MA. Fluorine-18: a new isotope for bone scanning. *J Nucl Med*. 1962;3:332-334

2- Schirrmeister H, Guhlmann A, Kotzerke J, et al. Early detection and accurate description of extent of metastatic bone disease in breast cancer with fluoride ion and positron emission tomography. *J Clin Oncol*. 1999;17:2381-2389

3- Raynor W, Houshmand S, Gholami S, et al. Evolving role of molecular imaging with 18F-sodium fluoride PET as a biomarker for calcium metabolism. *Curr Osteoporos Rep*. 2016;14:115-125

4- Adesanya O, Sprowson A, Masters J, Hutchinson C. Review of the role of dynamic 18F-NaF PET in diagnosing and distinguishing between septic and aseptic loosening in hip prosthesis. *J Orthop Surg Res*. 2015;16:10-15

5- Wilson GH 3rd, Gore JC, Yankeelov TE, et al. An approach to breast cancer diagnosis via PET imaging of microcalcifications using (18)F-NaF. *J Nuc Med*. 2014;55:1138-1143

6- Wu J, Zhu, H, Ji H. Unexpected detection of brain metastases by 18F-NaF PET/CT in a patient with lung cancer. *Clin Nucl Med*. 2013;38:429-432

7- Blomberg BA, de Jong PA, Thomassen A, et al. Thoracic aorta calcification but not inflammation is associated with increased cardiovascular disease risk:

results of the CAMONA study. *Eur J Nucl Med Mol Imaging*. 2017;44:249-258.

8- Fiz F, Morbelli S, Piccardo A, et al. 18F-NaF uptake by atherosclerotic plaque on PET/CT imaging: inverse correlation between calcification density and mineral metabolic activity. *J Nucl Med*. 2015;56:1019-1023

9- Derlin T, Toth Z, Papp L, et al. Correlation of inflammation assessed by 18F-FDG PET, active mineral deposition assessed by 18F-fluoride PET, and vascular calcification in atherosclerotic plaque: a dual-tracer PET/CT study. *J Nucl Med*. 2011;52:1020-1027

10- Asmar A, Simonsen L, Svolgaard B, et al. Unexpected diffuse 18F-NaF uptake in the lung parenchyma in a patient with severe hypercalcemia due to myelomatosis. *Clin Nucl Med*. 2017;42:68-69.

11- Shao F, Zou Y, Cai L, et al. Unexpected detection of urinary bladder cancer on dual phase 18F-NaF PET/CT in a patient with back pain. *Clin Nucl Med*. 2016;41:902-904.

12- Al-Zaghal A, Werner TJ, Høilund-Carlsen PF, Alavi A. The detection of uterine leiomyoma (fibroid) calcifications on 18F-NaF PET/CT. *Clin Nucl Med*. 2018; doi: 10.1097/RLU.0000000000002122

13- Saboury B, Ziai P, Alavi A. Detection and quantification of molecular calcification by PET/computed tomography: a new paradigm in assessing atherosclerosis. *PET clin.* 2011;6:409-415

14- Deng H, Zheng W, Jankovic J. Genetics and molecular biology of brain calcification. *Ageing Res Rev*. 2015;22:20-38

15- Grech R, Grech S, Mizzi A. Intracranial calcifications. A pictorial review. *Neuroradiol J*. 2012;25:427-451

16- Blomberg B.A., Thomassen A., Takx R.A.P, et al. Delayed 18F-fluorodeoxyglucose PET/CT imaging improves quantitation of atherosclerotic plaque inflammation: results from the CAMONA study. *J Nucl Cardiol*. 2014;21:588-597

17- D'Agostino Sr RB, Vasan RS, Pencina MJ, et al. General cardiovascular risk profile for use in primary care: the Framingham Heart Study. *Circulation*. 2008;117:743–753.

18- Blomberg BA, Thomassen A, de Jong PA, et al. Coronary fluorine-18-sodium fluoride uptake is increased in healthy adults with an unfavorable cardiovascular risk profile: results from the CAMONA study. *Nucl Med Commun*. 2017;38:1007-1014

19- Blomberg BA, Thomassen A, Takx RA, et al. Delayed sodium 18F-fluoride PET/CT imaging does not improve quantification of vascular calcification

metabolism: results from the CAMONA study. *J Nucl Cardiol*. 2014;21:293-304

20- Daghighi MH, Rezaei V, Zarrintan S, Pourfathi H. Intracranial physiological calcifications in adults on computed tomography in Tabriz. *Folia Morphol (Warsz)*. 2007;66:115-119

21- Kiroglu Y, Calli C, Karabulut N, Oncel C. Intracranial calcification on CT. *Diagn Interv Radiol*. 2010;16:263-269

22- Kendall B, Cavanagh N. Intracranial calcification in paediatric computed tomography. *Neuroradiology*. 1986;28:324-330.

23- Maslinska D, Laure-Kamionowska M, Deregowski K, Maśliński S. Association of mast cells with calcification in the human pineal gland. Folia *Neuropathol*. 2010;48:276-282

24- Zimmerman RA, Bilaniuk LT. Age-related incidence of pineal calcification detected by computed tomography. *Radiology*. 1982;142:659-662

25- Beall SS, Pattern BM, Mallette L, Jankovic J. Abnormal systemic metabolism of iron porphyrin, and calcium in Fahr's syndrome. *Ann Neurol*. 1989;569-575

26- Duckett S, Galle P, Escourolle R, Poirier J, Hauw JJ. Presence of zinc aluminum, magnesium in striopalledodentate (SPD) calcifications (Fahr's disease): electron probe study. *Acta Neuropathol*. 1977;38:7-10

27- Costeas A, Woodard HQ, Laughlin JS. Depletion of 18F from blood flowing through bone. *J Nucl Med*. 1970;11:43-45

28- Bastawrous S, Bhargava P, Behnia F, Djang DS, Haseley DR. Newer PET application with an old tracer: role of 18F-NaF skeletal PET/CT in oncologic practice. *Radiographics*. 2014;34:1295-1316

29- Grant FD, Fahey FH, Packard AB, Davis RT, Alavi A, Treves ST. Skeletal PET with 18F-fluoride: applying new technology to an old tracer. *J Nucl Med*. 2008;49;68-78.

30- Czernin J, Satyamurthy N, Schiepers C. Molecular mechanisms of bone 18F-NaF deposition. *J Nucl Med*. 2010;51:1826-9

31- Blake GM, Park-Holohan SJ, Cook GJ, Fogelman I. Quantitative studies of bone with the use of 18F-fluoride and 99mTc-methylene diphosphonate. *Semin Nucl Med*. 2001;31:28-49

32- Kwak R, Takeuchi F, Yamatomo N, Nakamura T, Kadoya S. Intracranial physiological calcification on computed tomography (part 2): calcification in the choroid plexus of the lateral ventricles. *No To Shinkei*. 1988;40:707-711

33- Whitehead MT, Oh C, Raju A, Choudhri AF. Physiologic pineal region, choroid plexus, and dural calcifications in the first decade of life. AJNR Am J *Neuroradiol*. 2015;36:575-580.

34- Yalcin A, Celyan M, Bayraktutan OF, Sonkaya AR, Yuce I. Age and gender related prevalence of intracranial calcifications in CT imaging; data from 12,000 healthy subjects. *J Chem Neuroanat*. 2016;78:20-24

35- Tapp E, Huxley M. The histological appearance of the human pineal gland from puberty to old age. *J Pathol*. 1972;108:137-144

36- Wu YW, Hess CP, Singhal NS, Groden C, Toro C. Idiopathic basal ganglia calcifications: an atypical presentation of PKAN. *Pediatr Neurol*. 2013;49:351-354

37- Go JL, Zee CS. Unique CT imaging advantages: hemorrhage and calcification. *Neuroimaging Clin N Am*. 1998;8:541-558

38- Atlas SW, Grossman RI, Hackney DB, et al. Calcified intracranial lesions: detection with gradient-echo-acquisition rapid MR imaging. *AJR Am J Roentgenol*. 1988;150:1383-1389

39- Livingston JH, Stivaros S, Van Der Knaap MS, Crow YJ. Recognizable phenotypes associated with intracranial calcification. *Dev Med Child Neurol*. 2013;55:46-57

40- Reichenbach JR, Schweser F, Serres B, Deistung A. Quantitative susceptibility mapping: concepts and applications. *Clin Neuroradiol*. 2015:25:225-230

41- Livingston JH, Stivaros S, Warren D, Crow YJ. Intracranial calcification in childhood: a review of aetiologies and recognizable phenotypes. *Dev Med Child Neurol*. 2014;56:612-622

42- Lago EG, Baldisserotto M, Hoefel Filho JR, Santiago D, Jungblut R. Agreement between ultrasonography and computed tomography in detecting intracranial calcifications in congenital toxoplasmosis. *Clin Radiol*. 2007;62:1004-1011

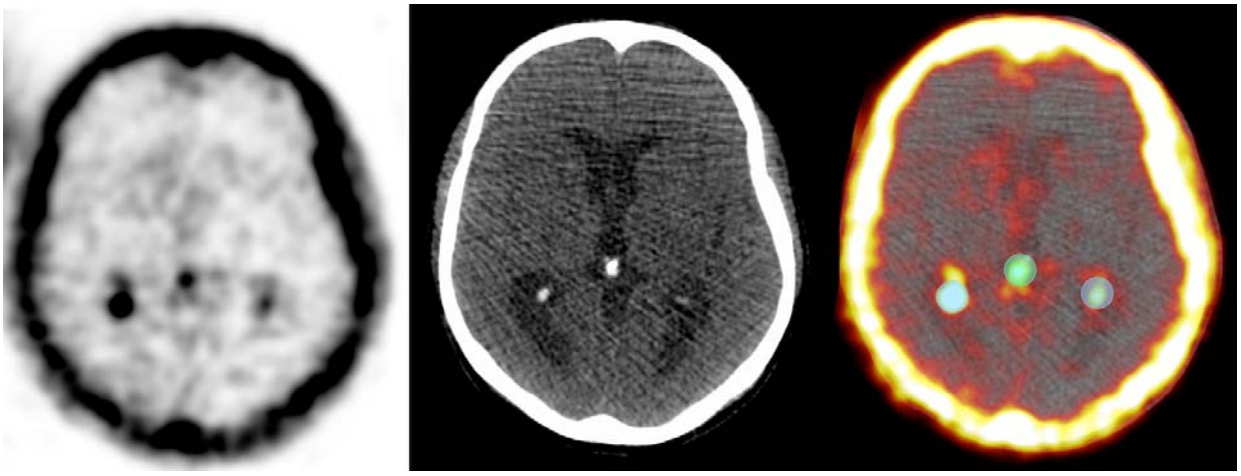

Figure 1. Axial PET, CT, and fused PET/CT brain images of a 59-year-old man illustrating the ROIs set over the calcified epithalamus and right and left choroid plexus. Mean NaF uptake and maximum HU were measured for each ROI.

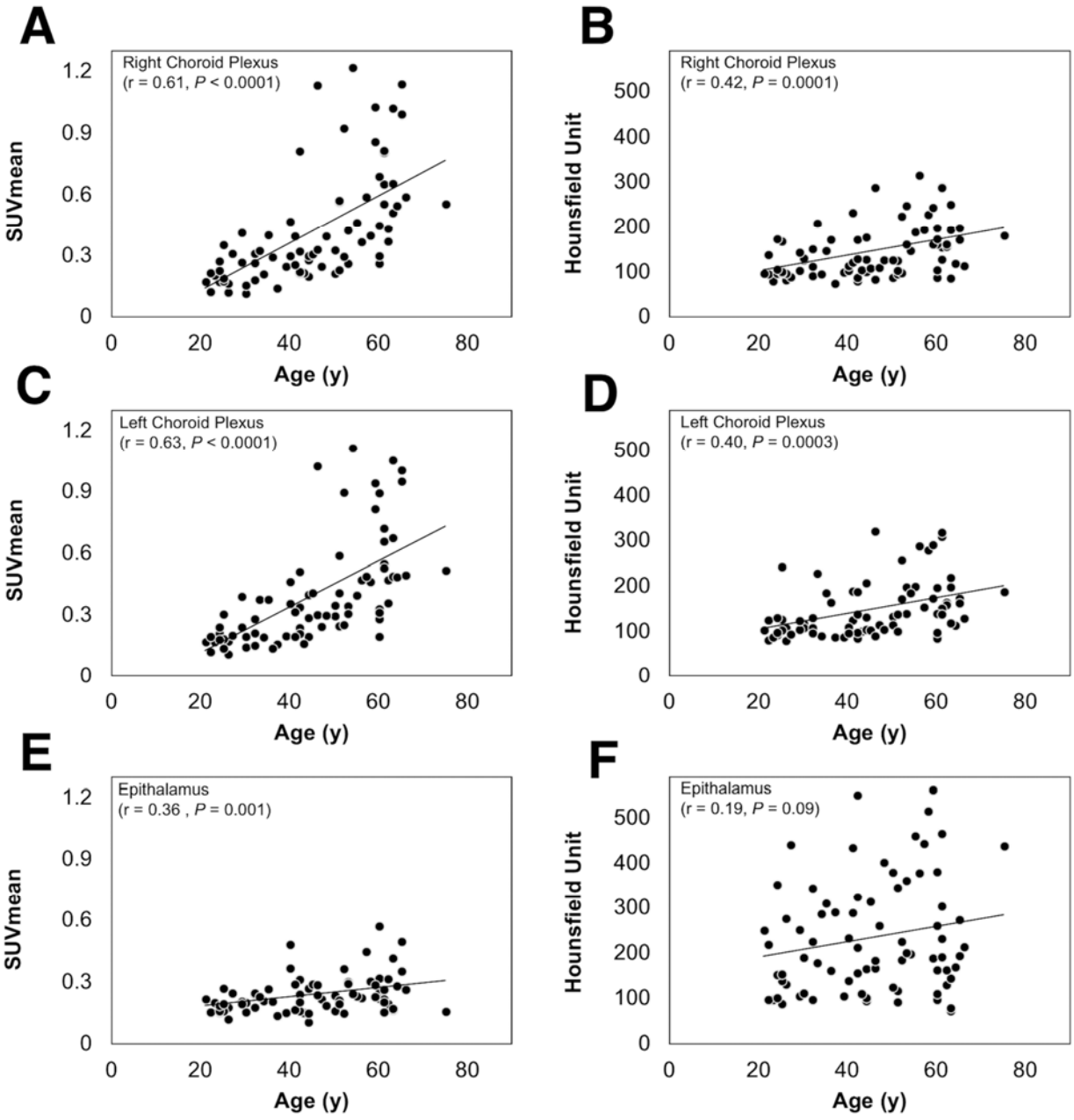

Figure 2. The correlation of NaF uptake (A, C, E) and maximum HU (B, D, F) in the choroid plexus and epithalamus with age.

r: Pearson's Correlation Coefficient
P: P-Value
SUVmean: Mean standardized uptake value

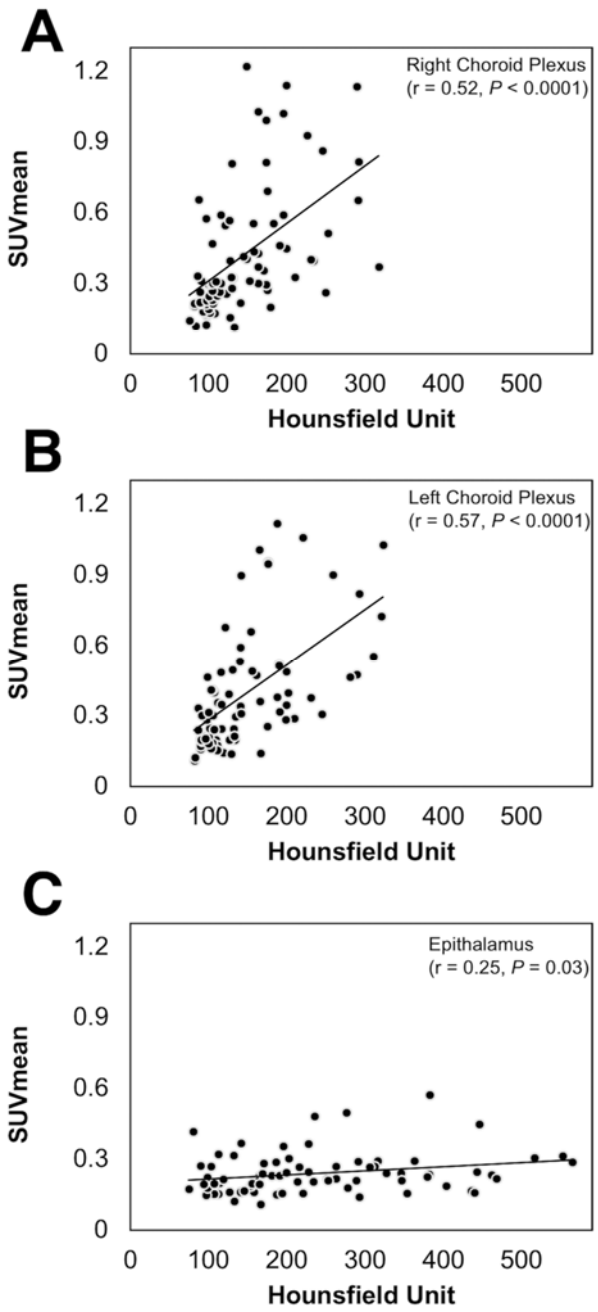

Figure 3. The correlations of NaF uptake with HU values in the right choroid plexus [A], left choroid plexus [B], and epithalamiums [C].

r: Pearson's Correlation Coefficient
P: P-Value
SUVmean: Mean standardized uptake value

Table 1. Subject Demographics

	Female (n=38)	Male (n=40)	P-Value	Total (N=78)
Age (Years)	45.28 ±14.56	45.27 ± 13.93	0.99	45.28 ± 14.15
BMI (Kg/m^2)	25.30 ± 3.12	27.57 ± 4.31	< 0.01	26.46 ± 3.92
BP (mm Hg)				
Systolic	124.75 ± 17.03	133.88 ± 16.91	0.02	129.43 ± 17.47
Diastolic	74.55 ± 10.39	78.61 ± 9.64	0.07	76.63 ± 10.15
Creatinine (mmol/L)	71.44 ± 9.97	87.72 ± 9.91	< 0.01	79.79 ± 12.83
MDRD-eGFR ($mL/min/1.73m^2$)	79.52 ± 13.66	83.72 ± 12.63	0.16	81.67 ± 13.23
Serum blood sugar (mmol/L)	5.36 ± 0.50	5.66 ± 0.43	< 0.01	5.51 ± 0.48
HbA1c (mmol/L)	33.05 ± 3.54	34.55 ± 4.56	0.10	33.82 ± 4.14
Fibrinogen (mmol/L)	9.20 ± 1.50	9.04 ± 1.37	0.63	9.12 ± 1.42
WBC ($10^9/L$)	5.79 ± 1.56	6.22 ± 2.14	0.28	5.99 ± 1.88
Triglyceride (mmol/L)	0.84 ± 0.30	1.26 ± 0.85	< 0.01	1.06 ± 0.67
Cholesterol (mmol/L)				
Total	4.99 ± 0.86	4.86 ± 0.87	0.50	4.92 ± 0.86
LDL	2.98 ± 0.79	3.11 ± 0.79	0.50	3.05 ± 79
HDL	1.69 ± 0.46	1.20 ± 0.29	< 0.01	1.44 ± 0.45
PET/CT systems				
GE Discovery STE	23	16		39
GE Discovery RX	8	17		25
GE Discovery 690/710	7	7		14
GE Discover VCT	0	0		0

Values are mean ± the standard deviation
MDRD-eGFR, glomerular filtration rate estimated by the Modification of Diet and Renal Disease formula
LDL, Low-Density Lipoprotein
HDL, High-Density Lipoprotein
BP, Blood Pressure
BMI, Body Mass Index

Supplemental Table 1. Point estimates (p-values) from multivariable analyses on all 6 endpoints after variance inflation factor analysis and backward variable selection (p_{stay}=0.7)

	Right choroid plexus		Left choroid plexus		Epithalamus	
	SUVmean (adj.R^2=0.40)	HU (adj.R^2=0.14)	SUVmean (adj.R^2=0.41)	HU (adj.R^2=0.08)	SUVmean (adj.R^2=0.15)	HU (adj.R^2=0.24)
Age (Years)	0.01 (<0.0001)	1.58 (0.002)	0.01 (<0.0001)	1.69 (0.007)	0.002 (0.001)	0.16 (0.89)
Male gender	-0.12 (0.11)	0.82 (0.96)	-0.06 (0.28)	-5.20 (0.82)	0.01 (0.59)	8.09 (0.84)
BMI (Kg/m^2)	-0.009 (0.29)	-0.97 (0.60)	-0.007 (0.36)	-1.47 (0.56)	0.004 (0.20)	-6.08 (0.17)
BP (mm Hg)						
Systolic		0.27 (0.51)	-0.002 (0.31)	0.19 (0.67)	-0.0005 (0.47)	2.46 (0.004)
Diastolic						
Creatinine (mmol/L)	0.002 (0.43)			-0.51 (0.52)	0.0006 (0.51)	1.36 (0.35)
MDRD-eGFR (mL/min/1.73m^2)						
Serum blood sugar (mmol/L)	0.06 (0.35)	6.21 (0.66)	0.04 (0.40)	15.75 (0.36)		35.39 (0.27)
HbA1c (mmol/L)				-1.24 (0.56)		9.17 (0.018)
Fibrinogen (mmol/L)			0.007 (0.67)	-2.28 (0.68)	0.009 (0.18)	-23.92 (0.022)
WBC (10^9/L)				2.09 (0.61)		14.81 (0.054)
Triglyceride (mmol/L)	0.11 (0.01)		0.10 (0.014)	9.85 (0.43)	0.007 (0.69)	-55.86 (0.017)
Cholesterol (mmol/L)						
Total						
LDL						-13.38 (0.44)
HDL	-0.06 (0.36)	-17.40 (0.31)	-0.05 (0.40)	-14.10 (0.47)		